



OPEN ACCESS

EDITED BY Peter Knittel.

Institute for Applied Solid State Physics (FHG), Germany

REVIEWED BY

Shingo Sotoma,

Kyoto Institute of Technology, Japan

Goutam Pramanik,

University Grants Commission Department of Atomic Energy Consortium for Scientific Research Kolkata Centre, India

*CORRESPONDENCE

Philip R. Hemmer, □ prhemmer@exchange.tamu.edu Masfer H. Alkahtani, ☑ mghtani@kacst.gov.sa

RECEIVED 18 August 2025 ACCEPTED 16 September 2025 PUBLISHED 25 September 2025

Alkahtani MH, Alzahrani YA, Hazrathosseini A, Alessa AM, Sow M, Alromaeh A, Alghihab AA, Alghannam FS, Jelezko F and Hemmer PR (2025) Advanced post-treatment strategy for quantum-grade fluorescent nanodiamonds. Front. Quantum Sci. Technol. 4:1687810. doi: 10.3389/frqst.2025.1687810

COPYRIGHT

© 2025 Alkahtani, Alzahrani, Hazrathosseini, Alessa, Sow, Alromaeh, Alghihab, Alghannam, Jelezko and Hemmer. This is an open-access article distributed under the terms of the Creative Commons Attribution License (CC BY)

The use, distribution or reproduction in other forums is permitted, provided the original author(s) and the copyright owner(s) are credited and that the original publication in this iournal is cited, in accordance with accepted academic practice. No use, distribution or reproduction is permitted which does not comply with these terms.

Advanced post-treatment strategy for quantum-grade fluorescent nanodiamonds

Masfer H. Alkahtani^{1*}, Yahya A. Alzahrani¹, Ayla Hazrathosseini², Abdulmalik M. Alessa¹, Maabur Sow³, Abdulaziz Alromaeh⁴, Abdulrahman A. Alghihab⁴, Faisal S. Alghannam⁵, Fedor Jelezko³ and Philip R. Hemmer^{2,6}*

¹Future Energy Technologies Institute, King Abdulaziz City for Science and Technology (KACST), Riyadh, Saudi Arabia, ²Institute for Quantum Science and Engineering, Texas A&M University, College Station, TX, United States, ³Institute for Quantum Optics, Ulm University, Ulm, Germany, ⁴Microelectronics and Semiconductors Institute, King Abdulaziz City for Science and Technology (KACST), Riyadh, Saudi Arabia, ⁵Next-Generation Connectivity and Wireless Sensors Institute, King Abdulaziz City for Science and Technology (KACST), Riyadh, Saudi Arabia, ⁶Department of Electrical and Computer Engineering, Texas A&M University, College Station, TX, United States

Fluorescent nanodiamonds (FNDs) containing nitrogen-vacancy (NV⁻) centers are promising platforms for quantum sensing and bioimaging, but their performance is often limited by surface defects, residual graphitic carbon, and ionic contamination. Here, we report a multistep surface treatment strategy combining molten potassium nitrate (KNO₃) thermal oxidation with sequential acid and alkaline cleaning to produce high-quality, quantum-grade FNDs. Molten KNO₃ etching at 580 °C enables morphological reshaping and partial oxidation, while subsequent H₂SO₄/HNO₃, NaOH, and HCl washes eliminate graphitic residues, neutralize surface charges, and remove metal ions. This protocol yields discrete, colloidally stable FNDs with enhanced photoluminescence, a high ODMR contrast of 11.5%, and extended average spin-lattice relaxation time $(T_1 \approx 2045 \ \mu s)$. Dynamic light scattering and ζ -potential measurements confirm excellent dispersion (~100 nm, -30 mV). The integration of chemical, morphological, and spin-performance improvements establishes a scalable route for producing FNDs suitable for high-fidelity quantum sensing and biophotonic applications.

KEYWORDS

fluorescent nanodiamonds, nitrogen-vacancy centers, surface post-treatment, spin coherence, quantum sensing

1 Introduction

Nanodiamonds (NDs) are carbon-based nanomaterials ranging from a few to several hundred nanometers in size, renowned for their exceptional mechanical hardness (Zhai et al., 2021; Fouda et al., 2022), high thermal conductivity (Wang et al., 2023; Kidalov, Shakhov, and Vul, 2007), chemical inertness (Kumar S. et al., 2019; Tegafaw et al., 2023), and excellent biocompatibility (Alkahtani et al., 2018b; Liu et al., 2022; Perevedentseva, Lin, and Cheng, 2021). These intrinsic properties make NDs attractive for a wide range of material and biomedical applications; however, their most technologically transformative feature is their ability to host optically active lattice defects, known as color centers, which emit across the ultraviolet (UV) to near-infrared (NIR) spectrum (Alkahtani et al., 2018b; Greentree et al., 2008; Aharonovich and Neu, 2014). Among these, the nitrogen-vacancy

(NV) center stands out as the most prominent and widely investigated defect in both bulk and nanoscale diamond. The NV center exhibits spin-dependent fluorescence at room temperature, enabling non-invasive optical readout of quantum spin states (Miller et al., 2020; Neumann et al., 2010; Pezzagna and Meijer, 2021; Katsumi et al., 2025). This quantum behavior, coupled with the robustness of the diamond host, positions FNDs as versatile platforms for next-generation technologies in quantum sensing (Alkahtani et al., 2018b; Katsumi et al., 2025; Alkahtani, Alzahrani, and Hemmer, 2023), nanoscale thermometry (Alkahtani et al., 2018c; Alkahtani Masfer et al., 2018; Alkahtani et al., 2017; Neumann et al., 2013; Kucsko et al., 2013), superresolution bioimaging (Gardill et al., 2022; Mosavian et al., 2024), and on-chip photonic and spintronic device engineering (Katsumi et al., 2025).

Commercially, NDs are produced through two dominant routes: bottom-up detonation synthesis, which yields ultrafine particles (<10 nm) from the shockwave decomposition of carbon-rich explosives (Volkov, Danilenko, and Elin, 1990; Panich et al., 2020), and top-down mechanical milling of high-pressure hightemperature (HPHT) single-crystal diamond into nanoscale fragments (Boudou et al., 2009; Stehlik et al., 2015). However, both synthesis routes inevitably generate substantial nondiamond content, including amorphous carbon, graphitic shells, metal, metal oxide residues, and aggregated debris (Volkov, Danilenko, and Elin, 1990; Boudou et al., 2009). These unwanted surface impurities adversely affect critical material properties. In particular, surface-bound sp² carbon and inorganic contaminants act as electronic and magnetic quenchers, reducing the brightness, photostability, and coherence times (T1 and T2) of NV centers (Sangtawesin et al., 2019; Dwyer et al., 2022; Peng, Dallas, and Takahashi, 2020). Consequently, precise post-synthetic purification and surface functionalization are essential for rendering NDs suitable for use in quantum and biomedical technologies (Tegafaw et al., 2023; Sangtawesin et al., 2019; Dwyer et al., 2022; Peng, Dallas, and Takahashi, 2020; Tsukahara et al., 2019).

Conventional purification strategies generally rely on oxidative treatments. Thermal oxidation in air or oxygen-rich atmospheres at 400 °C-600 °C removes superficial graphitic layers and introduces oxygen-containing functional groups (e.g., -COOH, -OH) that improve hydrophilicity and NV- charge state stability (Tsukahara et al., 2019; Bradac et al., 2013; Wolcott et al., 2014; Bradac and Osswald, 2018; Kumar R. et al., 2019; Hauf et al., 2011; Petráková et al., 2012). Alternatively, aggressive liquid-phase protocols employing concentrated acids such as H2SO4, HNO3, and HClO4 are commonly used to eliminate both organic and metallic residues (Schrand, Hens, and Shenderova, 2009; Brown et al., 2019). While effective, these methods suffer from extended processing times, harsh operating conditions, with significant safety and scalability limitations, making them suboptimal for high-throughput applications (Schrand, Hens, and Shenderova, 2009; Zhang et al., 2021; Fu et al., 2010).

Recently, molten nitrate-based oxidation, particularly using potassium nitrate (KNO₃), has emerged as a promising alternative. When applied at elevated temperatures (500 °C–600 °C), molten KNO₃ provides a highly oxidative medium capable of rapidly etching surface-bound sp² carbon and revealing crystallographic features such as etch pits aligned with the

{100} and {111} planes (Chu et al., 2014; Havlik et al., 2013; Alkahtani et al., 2018b; Zhang et al., 2017). This method facilitates a transformation of nanodiamond morphology from irregular, shard-like geometries into more uniform, rounded particles, improving colloidal behavior and reducing mechanical damage during milling processing. The low activation energy of this approach (~52 kJ/mol) further enables efficient etching compared to traditional gas-phase oxidations (Chu et al., 2014).

However, standalone KNO₃ etching remains insufficient for optical-grade nanodiamond purification. While it effectively removes most of the disordered carbon and reshapes the particle morphology, residues of partially oxidized graphitic domains and embedded nitrate salts can persist on the surface. Additionally, the presence of spin-active impurities, such as nitro oxides, can introduce spin noise, further affecting the coherence and optical properties of the embedded color centers. This spin noise may lead to reduced spin polarization and altered fluorescence, ultimately limiting the performance of nanodiamonds in quantum sensing applications (Barton et al., 2020).

To remove surface contaminants and enhance the optical spin performance of FNDs, residual nitrate salts and graphitic domains are eliminated via post-acid cleaning with concentrated sulfuric and nitric acids. This step also introduces hydrophilic –COOH and –OH groups. The acid-treated nanodiamonds are then washed with NaOH to neutralize residual acids, convert –COOH groups into –COO carboxylates, dissolve milling-derived metal ions (including potassium), and improve solubility. A final HCl treatment removes remaining alkali or transition metal contaminants and reprotonates the carboxylates to –COOH groups. This integrated protocol effectively eliminates impurities, improves colloidal stability and surface charge, and optimizes the optical properties of the nanodiamonds for high-performance applications.

To evaluate the physicochemical and quantum-optical evolution of FNDs at each stage, we employed a comprehensive suite of characterization tools. Transmission electron microscopy (TEM) was employed to evaluate morphological integrity and surface cleanliness, while dynamic light scattering (DLS) and zeta potential measurements were used to determine hydrodynamic size and assess colloidal stability. Optical microscopy combined with steady-state photoluminescence (PL) imaging enabled singleparticle fluorescence intensity tracking and photostability evaluation under continuous excitation. Furthermore, optically detected magnetic resonance (ODMR) measurements were performed to assess the continuous wave ODMR contrast and quantum coherence properties of NV centers. The optimized ND cleaning method we describe here is both scalable and environmentally sustainable, offering a robust pathway for the reliable production of high-purity, quantum-grade nanodiamonds tailored for advanced applications in quantum sensing, bioimaging, and nanophotonics.

2 Materials and methods

2.1 Materials

FNDs with a mean particle size of 100 nm (HPHT, Adámas Nanotechnologies, NC, USA) used as the starting material. Analytical grade potassium nitrate (KNO_3), sulfuric acid (H_2SO_4 ,

98%), nitric acid (HNO $_3$, 70%), sodium hydroxide (NaOH, pellets), and hydrochloric acid (HCl, 37%) were procured from Sigma-Aldrich. Ultrapure deionized (DI) water (resistivity $\geq 18.2~M\Omega \cdot cm$) was used for all cleaning and dispersion steps.

2.2 KNO₃ etching of nanodiamonds

In this step, 2 mg of FNDs were thoroughly mixed with 1 g of potassium nitrate (KNO $_3$) using a stainless-steel spatula to ensure homogeneous blending. The mixture was then subjected to thermal oxidative etching by heating in a ceramic crucible at 580 °C for 10 min under ambient atmospheric conditions Following the thermal etching, the sample was allowed to cool to room temperature, then dissolved in deionized water and centrifuged to pellet the nanodiamond particles. The resulting pellet was resuspended in 2 mL of water, sonicated for 10 s in an ultrasonic bath to disperse aggregates, and centrifuged again at 15,000 rpm for 10 min. This washing cycle was repeated five times to ensure the complete removal of soluble salt residues. After the final wash, the cleaned FND suspension was transferred to a glass vial and stored at room temperature for subsequent use in post-treatment and characterization steps.

2.3 Post-acid cleaning

To remove inorganic residues and oxidize surface carbon, the KNO₃-treated nanodiamonds were subjected to strong acid oxidation. A mixture of concentrated sulfuric acid and nitric acid (9:1 v/v) was used. The nanodiamond-KNO₃ composite was immersed in the acid mixture and stirred continuously at 75 °C for 72 h. This step facilitated removal of residual graphite and induced grafting of hydrophilic carboxyl (–COOH) and hydroxyl (–OH) groups at defect-rich regions. After cooling to room temperature, the suspension was diluted with DI water (pH = 6.5) and centrifuged at 12,000 rpm for 10 min. The supernatant was discarded and the pellet was retained for further washing.

2.4 Alkaline cleaning

The acid-treated nanodiamonds were resuspended in 0.1 M NaOH solution and heated at 90 °C for 2 h under constant stirring. This step served to neutralize residual acids, convert surface –COOH groups to their deprotonated –COO $^-$ form (enhancing solubility), and dissolve remaining potassium or other metal ions. After treatment, the dispersion was cooled, diluted with DI water (pH = 6.5), and centrifuged at 12,000 rpm for 10 min. The supernatant was discarded and the pellet was reserved for final cleaning.

2.5 Acid cleaning

To complete the purification, the nanodiamonds were treated with 0.1 M HCl at 90 $^{\circ}$ C for 2 h. This treatment effectively removed

residual metal cations (e.g., Fe2+, Cu2+) by converting them into soluble metal chlorides. The acidic environment during this step also transiently protonated surface carboxylate groups (-COO-) to -COOH; however, the final protonation state depends on the suspension pH after processing. After cooling, the suspension was diluted with DI water and centrifuged at 12,000 rpm for 10 min. The pellet was resuspended in DI water and adjusted to a neutral pH (6.5), resulting in partial deprotonation of-COOH groups in line with their pKa (~5). It is worth noting that we initially began the process with 2 mg of fluorescent nanodiamonds (FNDs) during the first step of molten KNO3 treatment. After completing all subsequent cleaning steps, 1.92 mg of the original material was successfully recovered, corresponding to a recovery yield of approximately 96%. This high recovery rate highlights the efficiency of the multistep treatment protocol in preserving the bulk of the FNDs while ensuring the effective removal of impurities and surface residues.

2.6 Dynamic light scattering (DLS) and zeta potential analysis

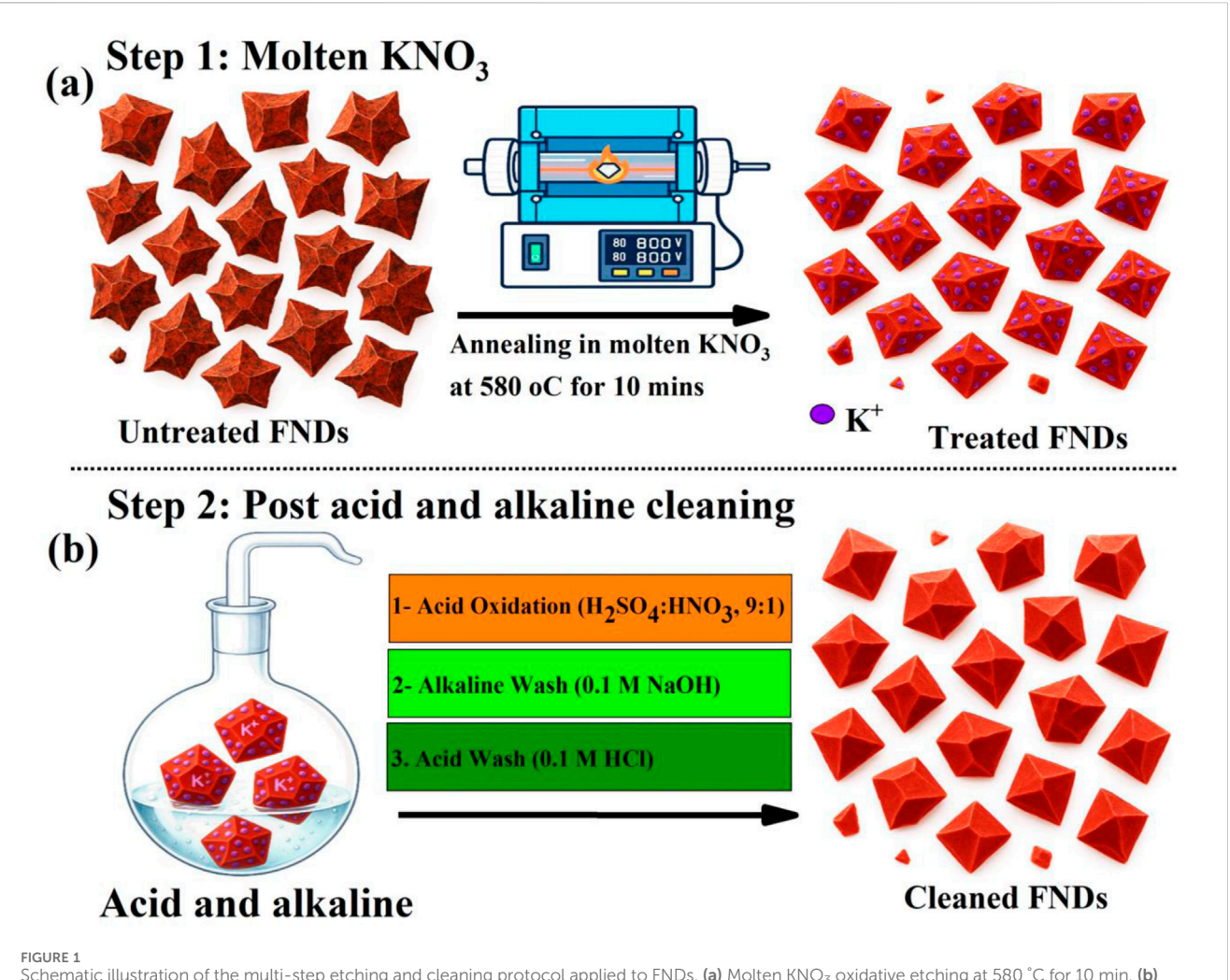
To evaluate the colloidal stability and size distribution of nanodiamonds after each cleaning step, dynamic light scattering (DLS) and ζ -potential measurements were performed using a Malvern Zetasizer Nano ZS instrument. For DLS, samples were diluted in DI water (pH = 6.5) to a concentration of ~0.01 mg/mL and filtered through a 0.22 μ m PTFE syringe filter prior to measurement. The hydrodynamic diameter and polydispersity index (PDI) were recorded at 25 °C. ζ -potential was measured using folded capillary cells (DTS1070) to assess the electrostatic stability of the suspensions. Values exceeding ± 30 mV were considered indicative of highly stable colloids.

2.7 Transmission electron microscopy (TEM)

Morphological characterization of the nanodiamonds was carried out using high-resolution transmission electron microscopy (HR-TEM, JEOL JEM-2100F). A drop of well-dispersed nanodiamond suspension was deposited onto carbon-coated copper grids and air-dried prior to imaging. Images were acquired under an accelerating voltage of 200 kV. Particle size, shape, edge roughness, and crystallinity were evaluated.

2.8 Confocal microscopy for optical measurements

The FNDs suspensions corresponding to the three treatment stages, (i) as-received FNDs, (ii) acid-cleaned FNDs, and (iii) KAA-treated FNDs, were each prepared at a concentration of 1 mg mL $^{-1}$. Equal volumes (10 μL) were drop-cast onto pre-cleaned quartz coverslips followed by spin-coating at 10,000 rpm for 10 s, ensuring identical deposited mass (~10 μg per coverslip). Fluorescence imaging and spot analysis were performed using a home-built confocal microscope equipped with a 532 nm continuous-wave excitation laser operated at 200 μW at the



Schematic illustration of the multi-step etching and cleaning protocol applied to FNDs. (a) Molten KNO_3 oxidative etching at 580 °C for 10 min. (b) Sequential post-treatment involving concentrated H_2SO_4/HNO_3 oxidation, followed by 0.1 M NaOH and 0.1 M HCl washes, eliminates residual inorganic salts and introduces hydrophilic surface functionalities (-COOH, -OH), thereby improving dispersion stability, surface charge, and optical properties.

sample plane and a high-numerical-aperture objective ($\times 100$, NA = 0.9). Photon collection was achieved using avalanche photodiodes through a 650 nm long-pass filter. All measurements were conducted under identical excitation and detection conditions, with fixed detector gain, integration times, and spectrometer settings to ensure quantitative comparability across samples.

2.9 Optically detected magnetic resonance (ODMR) and lifetime measurements

ODMR spectra were recorded under continuous-wave 532 nm laser excitation while sweeping a microwave field (2.7–3.0 GHz) using a signal generator connected to a coplanar waveguide. Fluorescence intensity was monitored synchronously to detect NV^- spin resonance dips. For spin-lattice relaxation time (T_1) measurements, a pulsed ODMR sequence was employed with variable delay times. Data were fitted to a stretched exponential decay model to extract T_1 values. All measurements were conducted at room temperature in ambient atmosphere.

3 Results

The multi-step etching and cleaning protocol employed in this study is schematically outlined in Figure 1. It integrates two complementary strategies: (i) molten potassium nitrate (KNO₃) oxidative etching, as previously described in (Chu et al., 2014; Havlik et al., 2013), and (ii) sequential acid and alkaline post-treatments adapted from established protocols (Huang and Chang, 2004). This combined approach is designed to overcome key limitations of conventional nanodiamond (ND) cleaning techniques, including poor photostability, low ODMR contrast, limited spin coherence times, and inadequate colloidal stability by simultaneously addressing surface-bound graphitic impurities and residual ionic contaminants.

Step 1 involves oxidative etching in molten KNO₃ at 580 °C for 10 min. As shown in Figure 1a, this treatment induces a notable morphological transition, converting the sharp, polyhedral geometries of as-received FNDs into more truncated, faceted structures with smoother edges. The high-temperature oxidative environment enhances surface accessibility and removes non-diamond carbon species. However, this step can also leave

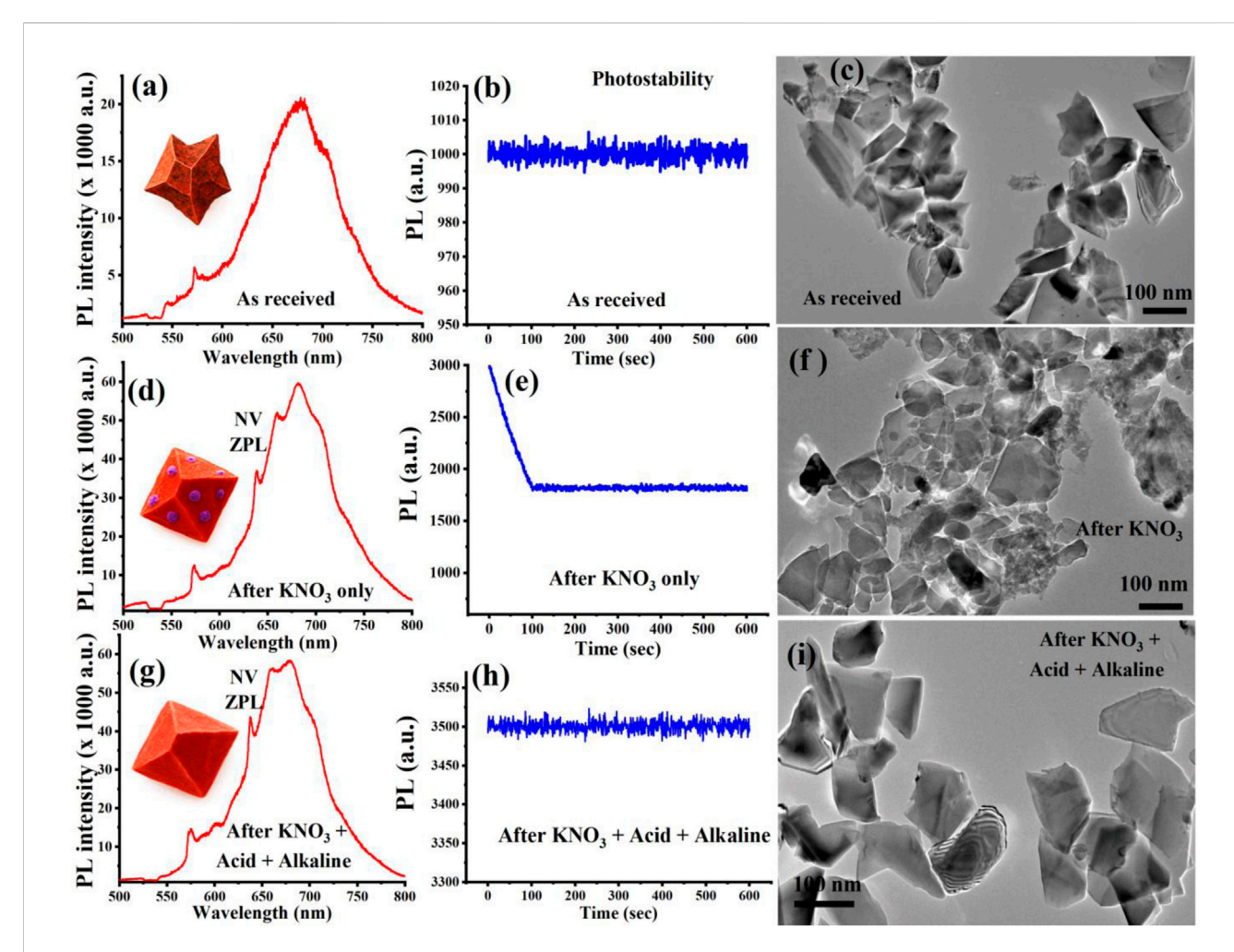


FIGURE 2
Optical and structural characterization of FNDs at each treatment stage. (a-c) As-received FNDs show broad PL emission, moderate photostability, and aggregated, rough particles. (d-f) KNO3-treated FNDs exhibit enhanced PL with clear NV ZPLs, reduced photostability, and partially sintered morphologies. (g-i) KAA-FNDs display strong, stable PL emission of an ensemble of NVs at a large excitation spot, well-dispersed nanodiamonds with smooth surfaces. The PL emission shown in (a, d, g) is from a single optical spot, representative of the ten spots tested at each cleaning stage.

behind potassium nitrate residues on some of the cleaned NDs at varying concentrations, which may affect the overall optical performance and disrupt the colloidal stability.

To restore optimal colloidal behavior and maximize optical performance, a sequential wet-chemical purification protocol was employed, consisting of concentrated H₂SO₄/HNO₃ oxidation followed by rinsing in 0.1 M NaOH and then in 0.1 M HCl, as illustrated in Figure 1b and detailed in the materials and methods section. The oxidative acid treatment serves as the primary cleaning step, aggressively removing residual sp²-carbon and amorphous carbon phases that quench NV center fluorescence, while simultaneously introducing oxygen-containing functionalities (-COOH, -OH, C=O) that increase surface polarity (Brown et al., 2019). Following the acid treatment, the KNO3-treated nanodiamonds were subjected to alkaline cleaning in a hot 0.1 M NaOH to neutralize residual acids, convert -COOH groups into their deprotonated -COO- form, and enhance solubility by dissolving remaining metal ions, including potassium. The NaOH treatment enhances the electrostatic surface charge, generating a high negative zeta potential that stabilizes the nanodiamonds in aqueous dispersion (Brown et al., 2019). The final step involves treatment with a hot 0.1 M HCl, which removes residual alkali or transition metal contaminants. In particular, potassium introduced during molten KNO₃ etching, partially removed by water washing but strongly adsorbed at oxygenated defect sites, remains on the surface until displaced in the HCl step. Proton exchange liberates K⁺ from surface coordination sites, while Cl⁻ complexes with K⁺ to form highly soluble KCl, ensuring its complete removal. This removal of tightly bound potassium and other ionic species helps maintain colloidal stability and reduces magnetic or charge spin noise near the nanodiamond surface (Barton et al., 2020), thereby preserving the optical performance of the NV centers in a wide range of promising applications.

To systematically evaluate the evolution of size, structure, and optical properties throughout the purification process, fluorescent nanodiamond (FND) samples were categorized into three distinct groups based on their treatment stage. The first group consists of asreceived FNDs, serving as the untreated control to establish baseline morphological and optical characteristics. The second group includes KNO₃-treated FNDs, which were subjected solely to

molten potassium nitrate oxidative etching at 580 °C for 10 min, enabling assessment of the effects of thermal oxidation on particle shape, surface purity, and photoluminescence behavior. The third and most refined group comprises KAA-FNDs (KNO₃–Acid–Alkaline) which represents FNDs that underwent the complete multi-step purification protocol, including molten KNO₃ etching followed by sequential acid ($\rm H_2SO_4/HNO_3$) and alkaline (NaOH, HCl) washing steps.

The optical and structural properties of the FND samples at each treatment stage were evaluated using a custom-built confocal laser scanning microscope and transmission electron microscopy (TEM). Representative results for photoluminescence (PL) emission, photostability, and particle morphology are presented in Figure 2. To enable a direct and quantitative comparison of optical measurements of the three treatment stages (as-received FNDs, acid-cleaned FNDs, and KAA-treated FNDs), confocal fluorescence scans were first performed to locate well-isolated regions with comparable emission intensities (Supplementary Figure S1). The excitation beam from a 532 nm continuous-wave laser was focused onto the sample using a $\times 100$ objective (NA = 0.9). All measurements were carried out under identical conditions, with a fixed excitation power of 200 μ W at the samples, the same detector gain and integration times. Photoluminescence spectra were acquired from optical spots of similar size and brightness, and each dataset was averaged over 10 such regions to improve statistical reliability.

As illustrated in Figure 2a, the as-received FNDs display a broad and unstructured PL emission spectrum centered around 680 nm, with weak or poorly resolved zero-phonon lines (ZPLs) associated with nitrogen-vacancy (NV-) centers. The PL spectrum was collected from one of the isolated optical spots, as shown in Supplementary Figure S1a, and is representative of the spectra obtained from other isolated spots, thereby verifying that the recorded emission is intrinsic to single FNDs and not influenced by aggregates. This spectral broadening is typical of nanodiamonds with surface contamination, such as graphitic shells or residual organics, which generate background fluorescence and mask the intrinsic NV⁻ emission. Nevertheless, as shown in Figure 2b, the asreceived FNDs exhibit relatively stable emission over time, photostability despite demonstrating moderate contaminated surfaces.

TEM analysis shown in Figure 2c further confirms the presence of significant particle aggregation, irregular shapes, and surface roughness, consistent with the presence of residual non-diamond carbon and incomplete surface passivation. These results highlight the need for rigorous post-synthesis purification to enhance both the optical performance and colloidal behavior of FNDs.

Following KNO₃ treatment, the FNDs display a pronounced enhancement in photoluminescence (PL) intensity together with a cleaner and more well-defined NV⁻ emission spectrum. This improvement, presented in Figure 2d, reflects the removal of surface impurities and non-diamond carbon that typically quench fluorescence. The spectrum was collected from one of the isolated optical spots, as shown in Supplementary Figure S1b, ensuring that the measured signal originates from individual nanodiamonds rather than aggregates, thereby providing a reliable representation of the intrinsic optical response after surface treatment. Distinct zero phonon lines (ZPLs) are clearly

observed at 575 nm (NV $^{\rm o}$) and 637 nm (NV $^{\rm o}$), indicating improved spectral definition and reduced background fluorescence. This enhancement is primarily attributed to the oxidative removal of surface graphitic carbon, which effectively exposes the diamond surface and mitigates non-radiative quenching pathways associated with sp $^{\rm 2}$ -bonded carbon domains. The elimination of these surface defects facilitates more efficient radiative recombination of NV centers, thereby boosting fluorescence output.

The optical improvement is accompanied by unexpected photobleaching, as shown in Figure 2e. This rapid photobleaching, even after meticulous cleaning, is particularly evident in KNO₃-treated FNDs. We attribute this behavior to the presence of fluorescent surface defects, which undergo gradual photobleaching, leaving behind only the NV center fluorescence. The corresponding TEM analysis shown in Figure 2f further supports this observation, revealing FND particles with partially rounded morphologies and residual surface contamination.

In contrast, the subsequent acid-alkaline washing step dramatically improves both optical and structural characteristics. As shown in Figure 2g, PL intensity further increases, reflecting more effective exposure and stabilization of NV⁻ centers due to the thorough removal of inorganic residues and passivation of reactive surface sites. This PL spectrum represents data collected from isolated optical spots, as shown in Supplementary Figure S1c, thereby ensuring that the measured emission originates from individual nanodiamonds rather than from aggregates. Notably, photostability is fully restored as illustrated in Figure 2h, indicating the elimination of charge-trapping impurities and suppression of photo-bleaching mechanisms. TEM imaging, as shown in Figure 2i, confirms these enhancements by revealing well-faceted, individually dispersed nanodiamonds with smooth surfaces and minimal aggregation. This morphology is indicative of successful surface reconstruction, effective removal of residual contaminants, and restored colloidal stability, validating the effectiveness of the complete KAA-FND purification protocol. To clearly demonstrate the impact of the sequential surface-cleaning steps, the PL spectra from all three treatment stages are compiled in Supplementary Figure S1d. This combined representation highlights the progressive enhancement in fluorescence intensity resulting from the removal of surface contaminants and the improved optical quality of the nanodiamonds. By presenting the spectra together, the figure provides a direct visual comparison that underscores the effectiveness of the surface treatments in producing brighter and more stable emitters.

To evaluate the quantum sensing potential of the treated FNDs, it was essential to investigate the spin relaxation dynamics of the nitrogen-vacancy (NV⁻) centers, particularly their longitudinal spin relaxation time (T₁), which reflects the decay of spin polarization back to thermal equilibrium. The T₁ relaxation time serves as a key figure of merit for quantum decoherence spectroscopy, especially in biological and ambient environments, where sensitivity to local magnetic noise is crucial (Barton et al., 2020; Nie et al., 2022; Wu et al., 2022). In the measurement protocol, NV centers were first optically polarized into the $|m_s=0\rangle$ sublevel of the 3A_2 ground state using a 1 μ s green laser pulse. After a variable delay, a second readout pulse was applied to monitor the population decay. As shown in Figures 3a,b, as-received FNDs exhibited a relatively short average T₁ of ~1045 μ s, measured across ten individual optical spots.

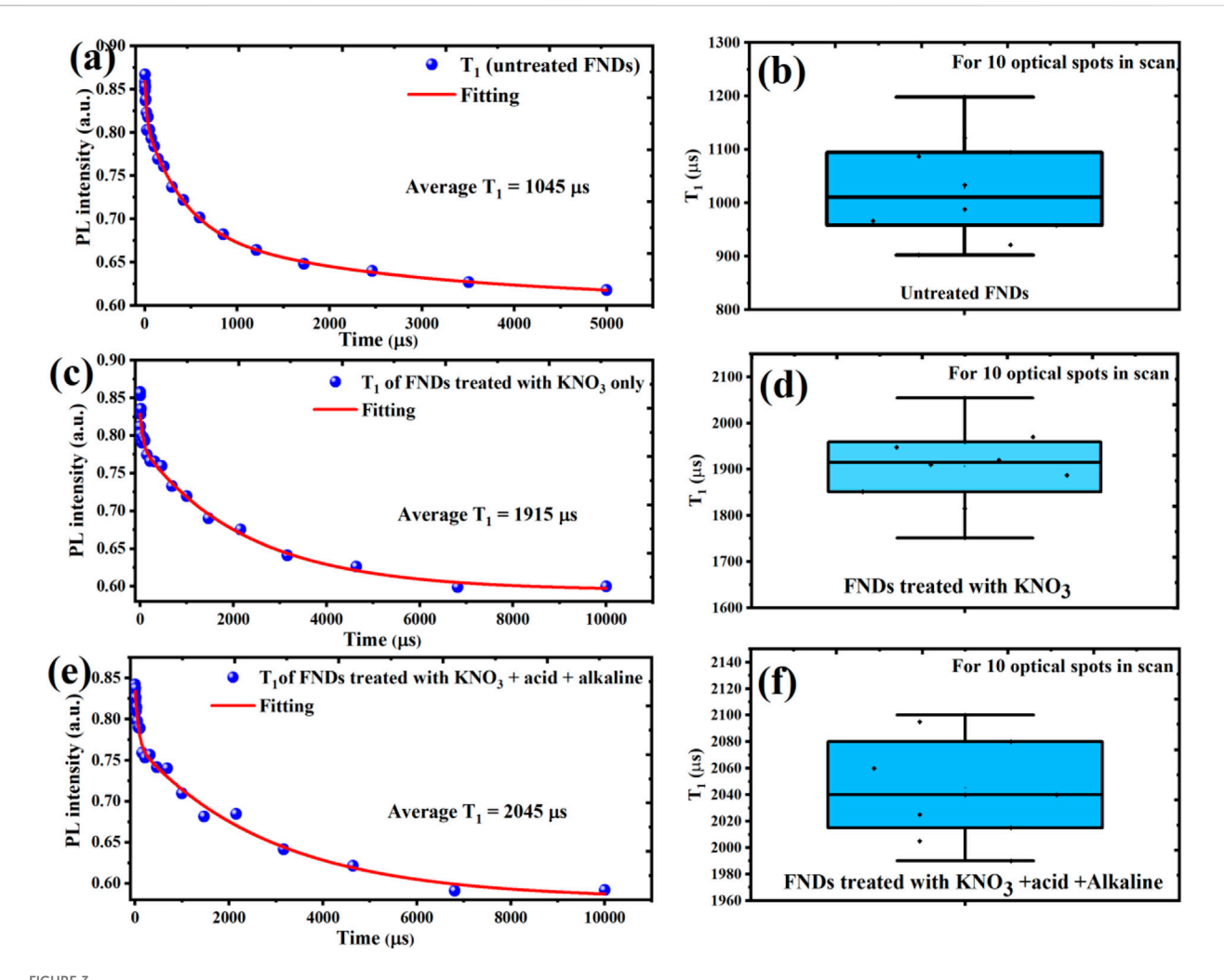
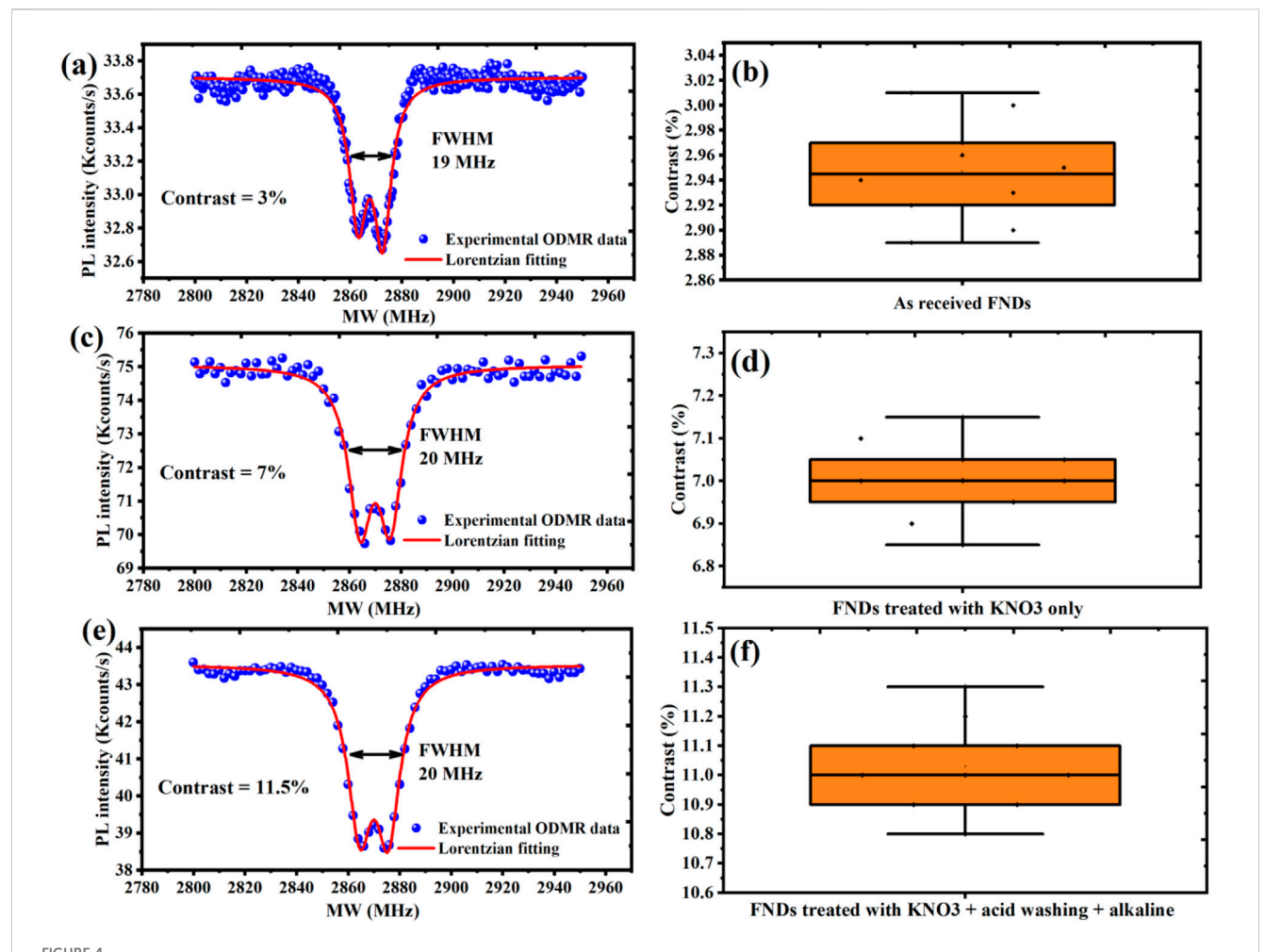


FIGURE 3 Spin relaxation measurements (T₁) of NV centers in FNDs at different purification stages averaged over 10 optical spots to ensure reproducibility. (a,b) As-received FNDs show short T₁ times (~1045 µs) due to surface spin noise and magnetic impurities. (c,d) KNO₃-treated FNDs exhibit improved T₁ (~1915 µs) from partial removal of graphitic and paramagnetic surface defects. (e,f) KAA-FNDs show the longest T₁ (~2045 µs), indicating effective elimination of ionic contaminants and surface trap states, resulting in enhanced spin coherence and quantum sensing readiness.

Such short relaxation times are consistent with the presence of surface spin noise, paramagnetic defects, and unpassivated dangling bonds, which act as fluctuating magnetic fields that accelerate spin decoherence. These results highlight the limitations of untreated nanodiamonds for high-fidelity quantum sensing and underscore the importance of surface purification for extending spin lifetimes.

Following KNO $_3$ treatment only, the T_1 relaxation time of the NV $^-$ centers show a clear increase, nearly doubling to ~1915 μ s, as presented in Figures 3c,d. This enhancement reflects a significant reduction in surface-associated magnetic noise, likely due to the partial removal of graphitic carbon layers and spin-active surface defects. By oxidatively etching away sp 2 -bonded carbon and some paramagnetic residues, the KNO $_3$ step reduces non-diamond surface states that typically accelerate spin relaxation. However, the presence of residual ionic contaminants, such as nitrate and potassium ions, continues to contribute to shallow trap states and local electric field fluctuations, which can still perturb spin coherence and limit T_1 extension (Barton et al., 2020).

The most pronounced improvement in spin relaxation is achieved after the full acid-alkaline treatment, where the average T_1 time reaches ~2045 µs, as shown in Figures 3e,f. This represents nearly a two-fold improvement compared to untreated FNDs and approaches the excellent T1 values reported for isolated single nanodiamonds with optimized surface conditions (March et al., 2023). The improved performance of the KAA-FNDs sample is reasonably associated with the reduction of residual metal ions, nitrate salts, and oxidized carbon impurities, together with the effective neutralization and passivation of the diamond surface. These treatments are expected to establish a cleaner, electronically quieter environment around the NV centers, reducing potential sources of decoherence such as fluctuating spins or electric dipoles. Although direct confirmation of complete ionic removal is not provided, the observed enhancements in T1 and ODMR contrast remain consistent with the advantages of comprehensive surface engineering in extending spin coherence and advancing the quantum sensing potential of nanodiamonds.



ODMR contrast of FNDs at different purification stages, averaged over 10 optical spots to ensure reproducibility. (a,b) As-received FNDs show low contrast (~3%) with high variability due to surface defects and charge instability. (c,d) KNO₃-treated FNDs exhibit improved contrast (~7%) with consistent enhancement across all measured spots. (e,f) KAA-FNDs achieve high contrast (~11.5%) with excellent reproducibility, confirming the effectiveness of the full purification protocol.

Given the critical role of ODMR in quantum sensing, nanoscale magnetometry, thermometry, and bioimaging, it is essential to evaluate the ODMR capabilities of our treated FNDs. This characterization not only verifies the suitability of the purified nanodiamonds for quantum applications but also reveals how surface chemistry directly impacts spin readout performance. Nitrogen-vacancy (NV-) centers in diamond serve as highly sensitive quantum probes capable of detecting local magnetic, electric, and thermal fluctuations at the nanoscale. Optically Detected Magnetic Resonance (ODMR) enables spin-state readout through fluorescence contrast and is among the most powerful techniques for quantum diagnostics. In a typical ODMR experiment, NV centers are first optically pumped into the $|m_s = 0\rangle$ sublevel of the triplet ground state using green laser excitation. A resonant microwave field then induces transitions to the $|m_s = \pm 1\rangle$ sublevels, causing a characteristic drop in fluorescence, measured as the ODMR dip. The depth of this dip, referred to as ODMR contrast, reflects both the crystal quality and the fidelity of spin readout. ODMR spectra for all three samples, presented in Figure 4, were acquired under 532 nm continuous-wave excitation while sweeping the microwave frequency from 2.7 to 3.0 GHz. As mentioned above, identical optical conditions (×100 objective, 200 μW laser power, fixed detector settings) were maintained for all measurements, and each spectrum represents an average over 10 comparable optical spots, as illustrated in Supplementary Figures S1a–c, to ensure reproducibility.

As shown in Figures 4a,b, as-received FNDs exhibit a relatively weak ODMR contrast of ~3%, primarily due to the presence of graphitic surface contamination, paramagnetic defects, and unstable NV charge states, which introduce non-radiative decay channels and parasitic background fluorescence. To ensure robust evaluation, ODMR data were collected from ten different optical spots across the sample, confirming the consistently low contrast typical of untreated FNDs. This baseline performance highlights the need for effective surface purification prior to quantum sensing applications.

For FNDs treated with KNO $_3$ only, the ODMR contrast increases significantly to \sim 7% as shown in Figures 4c,d, attributed to the oxidative removal of sp 2 -bonded carbon, which reduces background fluorescence and partially stabilizes NV $^-$ charge states. While this step improves signal clarity, residual ionic contaminants such as potassium and nitrate likely persist,

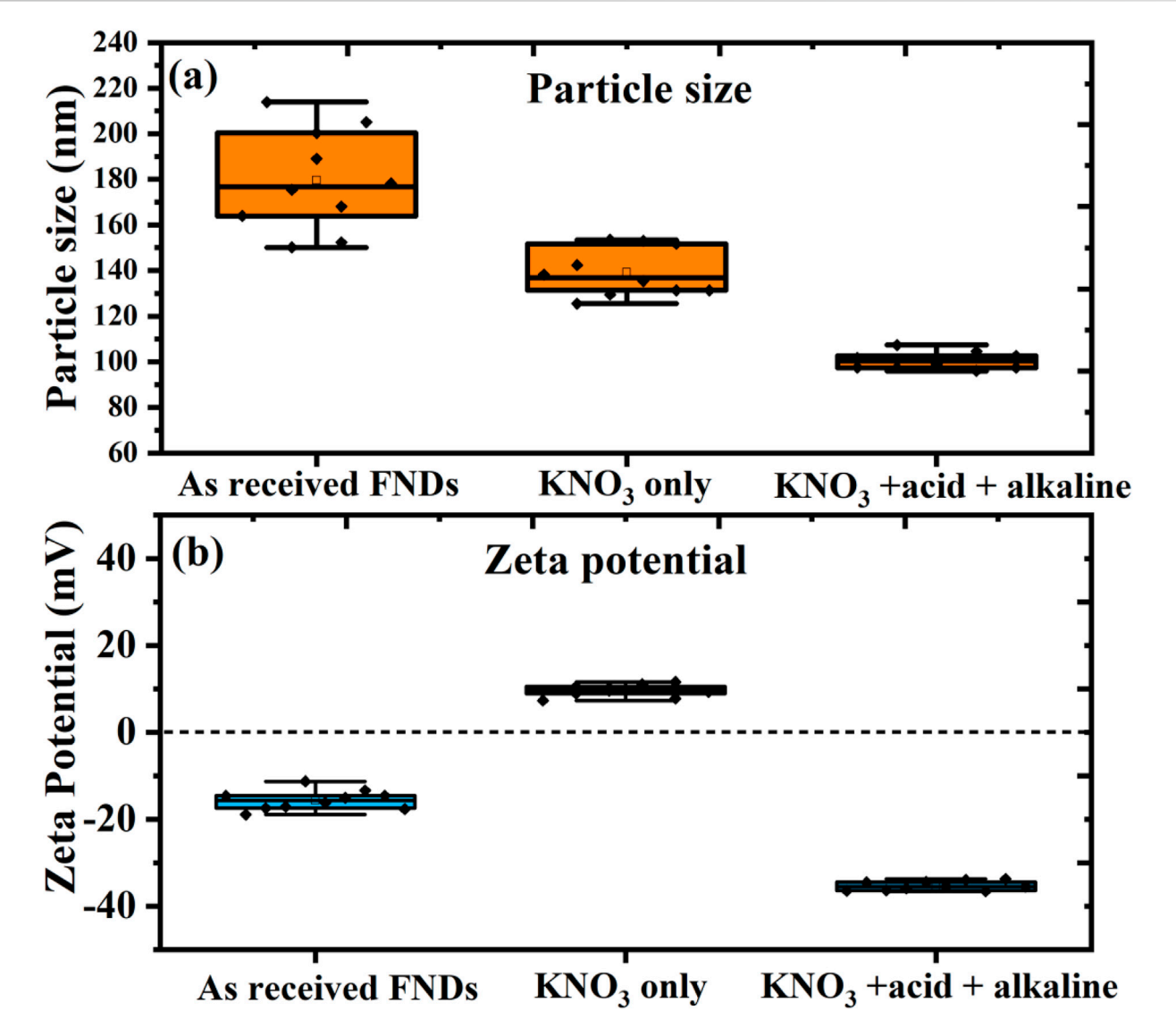


FIGURE 5
Colloidal stability and surface charge evolution of *filtered* FNDs during purification. (a) Hydrodynamic particle size distribution and (b) zeta potential of three FND groups: as-received FNDs (untreated), KNO₃-treated FNDs (oxidized in molten KNO₃ at 580 °C for 10 min), and KAA-FNDs (treated with molten KNO₃, followed by sequential acid and alkaline washing). As-received FNDs show broad size distribution (180–200 nm) and weak surface charge (–20 mV), indicating poor dispersion. KNO₃-treated FNDs exhibit reduced size (140 nm) but near-neutral surface potential (5 mV), limiting colloidal stability. In contrast, KAA-FNDs demonstrate monodispersity (100 nm) and strong surface charge (–30 mV), ensuring excellent electrostatic stability. Notably, KAA-FNDs retained dispersion without aggregation for over 3 months, confirming their long-term colloidal robustness.

introducing trap-assisted decoherence and local electric field noise. To validate this improvement, contrast measurements were repeated at ten spatially distinct positions, demonstrating a reproducible enhancement across the sample.

The best contrast enhancement occurred for KAA-FNDs sample, which undergo full acid-alkaline post-treatment, resulting in an ODMR contrast of ~11.5% as illustrated in Figures 4e,f. This performance gain is attributed to the comprehensive removal of ionic residues, complete surface neutralization, and passivation of dangling bonds, which together create an electronically stable environment for NV centers. To confirm the reliability of this result, ODMR measurements were statistically averaged over ten independent optical regions, all exhibiting consistently high contrast. The

bifurcation observed in the ODMR photoluminescence (PL) intensity dips in Figures 4a,c, and e originates from the intrinsic spin Hamiltonian of the NV $^-$ center in diamond. The NV $^-$ ground state is a spin triplet ($m_s=0,\pm 1$) with a zero-field splitting of $\sim\!2.87$ GHz. In the presence of local perturbations, the degeneracy of the $m_s=\pm 1$ sublevels is lifted, resulting in two distinct resonance conditions that appear as a split ODMR dip. This splitting has traditionally been attributed to strain fields in the nanodiamond lattice or weak external magnetic fields; however, recent studies demonstrate that local electric fields, most likely generated by nearby charged P1 centers, are the primary cause of zero-field ODMR splitting (Mittiga et al., 2018). Our findings align with this view, suggesting that the observed bifurcation arises from a combined influence of local electric

fields, donor-related impurities, and residual strain or magnetic perturbations within the FNDs.

The colloidal behavior of FNDs plays a vital role in enabling their performance in biological labeling, drug delivery, and fluid-phase quantum sensing. The colloidal behavior of FNDs plays a vital role in enabling their performance in biological labeling, drug delivery, and fluid-phase quantum sensing. Colloidal stability and surface charge evolution of FNDs during purification are shown in Figure 5 as follows: (a) hydrodynamic particle size distribution and (b) zeta potential of three FND groups: as-received FNDs (untreated), KNO₃-treated FNDs (oxidized in molten KNO₃ at 580 °C for 10 min), and KAA-FNDs (treated with molten KNO₃, followed by sequential acid and alkaline washing).

As-received FNDs show a broad size distribution (180–200 nm) and weak surface charge ($-20\,$ mV), indicating strong aggregation. The commercial supplier likely adds special dispersing agents to maintain particle dispersion in the original solvent. However, after removing the FNDs from the solvent, washing with DI water, and drying them for further use, these stabilizing agents are lost, leading to poor dispersion and the observed aggregation. The KNO3 treatment leads to partial oxidation and the removal of surface graphitic carbon, resulting in slightly smaller particle sizes (140 nm). However, the particles remain poorly dispersed due to near-neutral surface charge (5 mV), limiting colloidal stability and maintaining a degree of aggregation.

Following the KNO₃ treatment, the KAA-FNDs undergo a sequential acid and alkaline washing process that effectively removes ionic contaminants and residual graphitic shell material. This treatment improves surface chemistry by introducing functional groups that enhance electrostatic interactions, resulting in a stronger negative surface charge (–30 mV) and improved colloidal stability. The washing steps also contribute to the size reduction of the particles to 100 nm, which is primarily due to the removal of amorphous carbon and the optimization of particle dispersion.

Notably, the KAA-treated fluorescent nanodiamonds (KAA-FNDs) exhibited remarkable long-term colloidal stability, maintaining uniform dispersion without visible aggregation or sedimentation for over 3 months. This stability is confirmed by Supplementary Figure S2, which combines DLS size distribution profiles with corresponding vial photographs. The DLS data show that the hydrodynamic size remained narrowly distributed, with only a minor peak shift from ~100 nm to ~105 nm over time, indicating minimal particle growth or clustering. Complementary photographs of the suspensions at one, two, and 3 months further demonstrate the absence of sedimentation, with the samples remaining optically homogeneous and free of macroscopic aggregates. Together, these results provide strong evidence for the robustness of the KAA treatment in preserving colloidal stability over extended storage periods.

4 Discussion

The performance of nitrogen-vacancy (NV⁻) containing FNDs is not only governed the diamond purity but also by their surface shape and chemistry, which directly affects their photophysical, spin, and colloidal properties. To contextualize the efficacy of our

multi-step purification protocol, we compare it with a broad spectrum of surface treatment methodologies reported in prior studies (Table 1). These include air oxidation, acid etching, molten salt oxidation, salt-assisted air oxidation (SAAO), and surface doping strategies, each with distinct advantages and limitations in terms of scalability, surface purity, and application readiness.

As illustrated in Table 1, for morphological and optical Improvements, our study demonstrates that molten KNO₃ oxidation alone (KNO₃-FNDs) significantly enhances photoluminescence (PL) intensity and spectral definition, consistent with reports by (Chu et al., 2014; Havlik et al., 2013; Hui et al., 2019), who observed similar brightness boosts and smoother morphologies following short-duration thermal treatments. This is primarily attributed to the removal of sp² carbon layers, which otherwise quench NV emission through non-radiative pathways. However, the molten salt approach also introduces residual ionic contaminants (e.g., K⁺, NO₃⁻), which, as noted in our study, contribute to poor photophysical properties and colloidal instability.

In contrast, air oxidation treatments, widely adopted for their simplicity and scalability reported for example, in (Tsukahara et al., 2019; Bradac and Osswald, 2018; Kumar R. et al., 2019) have been shown to modestly improve PL and stabilize NV⁻ charge states, but often fail to remove deeply embedded graphitic or inorganic impurities. Furthermore, these methods generally retain sharp faceting and yield limited improvements in colloidal or spin properties.

Acid treatment protocols such as those explored by (Schrand, Hens, and Shenderova, 2009; Brown et al., 2019) are effective at oxidizing surface-bound carbon and enhancing hydrophilicity, but alone do not sufficiently improve PL brightness or NV spin readout due to the persistence of non-diamond carbon or insufficient defect passivation. Our multi-step KAA-FND approach (KNO3-acid-alkaline) synergistically combines the etching power of molten KNO3 with the chemical precision of wet acid and alkaline neutralization. This results in FNDs with high brightness, strong and stable NV $^-$ zero phonon lines (ZPLs), and excellent colloidal dispersion, outperforming all single-step treatments.

As for spin coherence and relaxation enhancement, spin relaxation time (T₁), a critical parameter for quantum sensing applications, serves as a sensitive probe of surface-induced magnetic noise. Our results show a progressive improvement in T₁ from ~1045 μs in as-received FNDs to ~1915 μs following KNO₃ etching, and up to ~2045 µs after the full KAA treatment. These enhancements are comparable to T₁ values reported in high-purity NDs treated via aerobic oxidation (Tsukahara et al., 2019) and reflect significant suppression of surface paramagnetic centers. Notably, molten KNO₃ alone improves T₁ through sp² carbon removal, similar to findings by Zhang et al. (2017), Hui et al. (2019). However, only the full KAA protocol yields spin coherence values approaching the theoretical limit for ensemble NVs in nanodiamonds (March et al., 2023), confirming the importance of ionic decontamination and chemical passivation in reducing noise near the NV center.

Optically Detected Magnetic Resonance (ODMR) contrast is a key figure of merit for quantum sensing, as it directly correlates with the fidelity of spin-state readout. The as-received FNDs exhibit weak contrast (~3%), consistent with the literature (Wolcott et al., 2014;

TABLE 1 Comparative summary of nanodiamond surface treatment strategies reported in the literature and this study. The table highlights the process conditions, resulting surface morphology, optical and spin properties.

Treatment Type	Process Conditions	Surface Morphology	Optical Properties	Spin Properties	Study/ References
Air Oxidation	Air, 500 °C-600 °C, several hours	Faceted, slight oxidation	Improved PL, NV ⁻ stabilized	T ₂ extended, noise reduced	Tsukahara et al. (2019)
Air Oxidation	Air annealing	Faceted; minimal change	Charge state shift (NV ⁰	Not reported	Bradac and Osswald, (2018)
Air Oxidation	Air oxidation, 500 °C–600 °C	Oxidized surface; retained shape	Stable PL	Not reported	Wolcott et al. (2014)
Air Oxidation	Controlled air oxidation	Faceted; size down to 1 nm	N/A	Not reported	Stehlik et al. (2015)
Air Oxidation	Air, variable oxidation	Faceted; oxidation dependent	PL enhanced by functionalities	Not reported	Kumar R. et al. (2019)
Air Oxidation	Selective air oxidation	Unchanged	NV ⁰ to NV ⁻ conversion	Not reported	Fu et al. (2010)
Acid Treatment	HNO ₃ /H ₂ SO ₄ /HClO ₄	Faceted; oxidized surface	Improved dispersion	Not reported	Brown et al. (2019)
Acid Treatment	Chemical polishing	Smoothened facets	N/A	N/A	Cherian et al. (1997)
Molten Salt (KNO ₃)	KNO ₃ , 500 °C-600 °C, short time	Rounded, bright surface	Boosted PL brightness	Not reported	Havlik et al. (2013)
Molten Salt (KNO ₃)	KNO ₃ etching	Rounded particles	Shape-dependent effects	Not reported	Chu et al. (2014)
Molten Salt (KNO ₃)	KNO ₃ annealing	Rounded, smooth edges	Anchoring behavior affected	Not reported	Zhang et al. (2017)
Molten Salt (KNO ₃)	Embedded polymer films	Clean, rounded	Stable PL, thermometry	Used for NV thermometry	Hui et al. (2019)
Salt-Assisted Air Oxidation	NaCl + air @ 500 °C	Rounded, clean	N/A	Not reported	Zhang et al. (2021)
Doping/Surface Engineering	Boron doping + SiV	Faceted with B/SiV defects	Strong SiV emission	Not reported	Alkahtani, (2023)
Molten Salt + Acid/ Alkaline	KNO ₃ @ 580 °C, 10 min + H ₂ SO ₄ / HNO ₃ , NaOH/HCl washes	Faceted, smooth, well-dispersed	Strong, stable PL; clear NV ZPLs	T ₁ ~2045 μs, high ODMR contrast (~11.5%)	This Study (KAA-FND)

Bradac and Osswald, 2018) and indicative of unstable NV charge states and surface quenching. KNO₃ etching improves ODMR contrast to ~7% through partial surface purification, echoing prior molten salt studies that reported enhanced optical quality without directly measuring spin performance.

The highest contrast (~11.5%) was obtained in our KAA-FNDs, surpassing previously reported values for ensemble NV systems and highlighting the critical importance of chemical neutralization in eliminating trap states and restoring NV charge stability. These results fill an existing gap in the literature, where ODMR characterization is often absent or limited to single-step treatments.

As for colloidal stability and surface charge, effective colloidal dispersion is vital for applications involving biological delivery, fluid-phase magnetometry, and sensor integration. Among previously reported treatments, only acid-cleaned or doped FNDs (Havlik et al., 2013; Schrand, Hens, and Shenderova 2009; Alkahtani 2023) addressed colloidal behavior explicitly, with mixed outcomes. Our zeta potential and DLS measurements demonstrate that only the KAA-treated FNDs achieve long-term stability, with a narrow size distribution (100 nm) and strong surface charge (–30 mV), ensuring aggregation-free dispersion for over 3 months. In contrast, KNO₃-treated particles exhibited poor zeta potential (~+5 mV), confirming the necessity of the post-treatment step for colloidal stabilization. By integrating insights from prior studies with our

systematic multi-step purification approach, we establish that the KAA-FND protocol offers a robust, scalable route to producing high-quality nanodiamonds with superior optical brightness, long spin coherence, strong ODMR contrast, and excellent colloidal stability. These features are critical for advancing the use of FNDs in quantum sensing, bioimaging, and nanoscale diagnostics.

Future work could combine this purification strategy with targeted doping or surface patterning to further enhance NV center functionality. Doping with elements such as silicon or phosphorus could improve sensitivity and coherence, while surface activation techniques, such as self-assembled monolayers, could offer precise control over surface functionalization and shape, enabling tailored applications in quantum computing, biomedicine, and advanced sensing technologies.

5 Conclusion

In this work, we have established a robust and scalable surface purification strategy for FNDs by integrating molten potassium nitrate (KNO $_3$) oxidative etching with sequential acid and alkaline post-treatments. This multi-step KAA-FND protocol addresses critical limitations of existing methods—including incomplete removal of graphitic carbon, residual ionic contamination, unstable NV $^-$ charge

states, and poor colloidal behavior-by enabling simultaneous morphological refinement, surface decontamination, and functional passivation. The resulting FNDs exhibit substantial enhancements across all key performance metrics: a marked increase in photoluminescence brightness with restored spectral definition and photostability; a near twofold improvement in spin-lattice relaxation time ($T_1 \approx 2045 \mu s$), reflecting reduced surface magnetic noise; a reproducibly high ODMR contrast reaching ~11.5%, indicative of stable NV- charge environments; and excellent colloidal stability with a narrow hydrodynamic size distribution (100 nm) and a strongly negative zeta potential (-30 mV). These synergistic optical, spin, and dispersion improvements position KAA-FNDs among the highest-performing nanodiamond materials reported to date. Importantly, our comparative analysis with air oxidation, acid-only, and molten salt-based treatments reveals that the inclusion of ionic neutralization and passivation steps is essential for achieving quantumgrade performance. This protocol thus offers a chemically rational, reproducible, and scalable route for engineering nanodiamond surfaces, enabling their deployment in high-precision quantum sensing, bioimaging, and next-generation quantum technologies.

Data availability statement

The original contributions presented in the study are included in the article/Supplementary Material, further inquiries can be directed to the corresponding authors.

Author contributions

MA: Methodology, Data curation, Formal Analysis, Supervision, Investigation, Funding acquisition, Conceptualization, Writing – review and editing, Writing – original draft. YA: Writing – original draft, Methodology, Data curation, Writing – review and editing, Software, Formal Analysis, AH: Data curation, Writing – review and editing, Formal Analysis, Methodology. AAe: Writing – original draft, Formal Analysis, Data curation, Methodology. MS: Software, Investigation, Writing – review and editing, Data curation, Methodology, Writing – original draft, Formal Analysis, AAr: Writing – original draft, Formal Analysis, Methodology, Data curation. AAg: Methodology, Writing – original draft, Formal Analysis, Data curation. FA: Writing – original draft. FJ: Data curation, Conceptualization, Investigation, Writing – review and editing, Formal Analysis, Writing – original draft. PH: Funding acquisition, Conceptualization, Project administration, Resources, Formal Analysis,

Writing – review and editing, Methodology, Supervision, Data curation, Writing – original draft.

Funding

The author(s) declare that financial support was received for the research and/or publication of this article. We acknowledge the support of King Abdelaziz City for Science and Technology (KACST), Saudi Arabia. PH acknowledges the support of NSF grant 2032567. This material is based upon work supported by the Air Force Office of Scientific Research under award number FA9550-23-1-0436.

Conflict of interest

The authors declare that the research was conducted in the absence of any commercial or financial relationships that could be construed as a potential conflict of interest.

Generative AI statement

The author(s) declare that no Generative AI was used in the creation of this manuscript.

Any alternative text (alt text) provided alongside figures in this article has been generated by Frontiers with the support of artificial intelligence and reasonable efforts have been made to ensure accuracy, including review by the authors wherever possible. If you identify any issues, please contact us.

Publisher's note

All claims expressed in this article are solely those of the authors and do not necessarily represent those of their affiliated organizations, or those of the publisher, the editors and the reviewers. Any product that may be evaluated in this article, or claim that may be made by its manufacturer, is not guaranteed or endorsed by the publisher.

Supplementary material

The Supplementary Material for this article can be found online at: https://www.frontiersin.org/articles/10.3389/frqst.2025.1687810/full#supplementary-material

References

Aharonovich, I., and Neu, E. (2014). Diamond nanophotonics. Adv. Opt. Mater. 2 (10), 911–928. doi:10.1002/adom.201400189

Alkahtani, M. (2023). Silicon vacancy in boron-doped nanodiamonds for optical temperature sensing. *Materials* 16 (17), 5942. doi:10.3390/ma16175942

Alkahtani, M., Jiang, L., Brick, R., Hemmer, P., and Scully, M. (2017). Nanometer-scale luminescent thermometry in bovine embryos. *Opt. Lett.* 42 (23), 4812–4815. doi:10.1364/OL. 42.004812

Alkahtani, M., Cojocaru, I., Liu, X., Herzig, T., Meijer, J., Küpper, J., et al. (2018a). Tinvacancy in diamonds for luminescent thermometry. *Appl. Phys. Lett.* 112 (24), 241902. doi:10.1063/1.5037053

Alkahtani, M. H., Alghannam, F., Jiang, L., Almethen, A., Rampersaud, A. A., Brick, R., et al. (2018b). Fluorescent nanodiamonds: past, present, and future. *Nanophotonics* 7 (8):1423–1453. doi:10.1515/nanoph-2018-0025

Alkahtani, M. H., Alghannam, F., Jiang, L., Rampersaud, A. A., Brick, R., Gomes, C. L., et al. (2018c). Fluorescent nanodiamonds for luminescent thermometry in the biological transparency window. *Opt. Lett.* 43 (14), 3317–3320. doi:10.1364/OL.43.003317

Alkahtani, M. H., Alzahrani, Y. A., and Hemmer, P. R. (2023). Engineering sub-10 nm fluorescent nanodiamonds for quantum enhanced biosensing. *Front. Quantum Sci. Technol.* 2, 1202231. doi:10.3389/frqst.2023.1202231

Barton, J., Gulka, M., Tarabek, J., Mindarava, Y., Wang, Z., Schimer, J., et al. (2020). Nanoscale dynamic readout of a chemical redox process using radicals coupled with nitrogen-vacancy centers in nanodiamonds. ACS Nano 14 (10), 12938–12950. doi:10. 1021/acsnano.0c04010

- Boudou, J.-P., Curmi, P. A., Jelezko, F., Wrachtrup, J., Aubert, P., Sennour, M., et al. (2009). High yield fabrication of fluorescent nanodiamonds. *Nanotechnology* 20 (23), 235602. doi:10.1088/0957-4484/20/23/235602
- Bradac, C., and Osswald, S. (2018). Effect of structure and composition of nanodiamond powders on thermal stability and oxidation kinetics. *Carbon* 132, 616–622. doi:10.1016/j.carbon.2018.02.102
- Bradac, C., Gaebel, T., Pakes, C. I., Say, J. M., Zvyagin, A. V., and Rabeau, J. R. (2013). Effect of the nanodiamond host on a nitrogen-vacancy color-centre emission state. *Small* 9 (1), 132–139. doi:10.1002/smll.201200574
- Brown, K. J., Chartier, E., Sweet, E. M., Hopper, D. A., and Bassett, L. C. (2019). Cleaning diamond surfaces using boiling acid treatment in a standard laboratory chemical hood. *J. Chem. Health and Saf.* 26 (6), 40–44. doi:10.1016/j.jchas.2019.06.001
- Cherian, K. A., Litster, J., Rudolph, V., and White, E. T. (1997). Chemical etching of diamond revisited: past basic research as guide to new processing technologies. *MRS Online Proc. Libr.* 495 (1), 419–424. doi:10.1557/PROC-495-419
- Chu, Z., Zhang, S., Zhang, B., Zhang, C., Fang, C.-Y., Rehor, I., et al. (2014). Unambiguous observation of shape effects on cellular fate of nanoparticles. *Sci. Rep.* 4 (1), 4495. doi:10.1038/srep04495
- Dwyer, Bo L., Rodgers, L. V. H., Urbach, E. K., Bluvstein, D., Sangtawesin, S., Zhou, H., et al. (2022). Probing spin dynamics on diamond surfaces using a single quantum sensor. *PRX Quantum* 3 (4), 040328. doi:10.1103/PRXQuantum.3.040328
- Fouda, S. M., Gad, M. M., Ellakany, P., Al Ghamdi, M. A., Khan, S. Q., Akhtar, S., et al. (2022). Flexural properties, impact strength, and hardness of nanodiamond-modified PMMA denture Base Resin. *Int. J. Biomaterials* 2022 (1), 1–10. doi:10.1155/2022/6583084
- Fu, K.-M. C., Santori, C., Barclay, P. E., and Beausoleil, R. G. (2010). Conversion of neutral nitrogen-vacancy centers to negatively charged nitrogen-vacancy centers through selective oxidation. *Appl. Phys. Lett.* 96 (12), 121907. doi:10.1063/1.3364135
- Gardill, A., Kemeny, I., Li, Y., Zahedian, M., Cambria, M. C., Xu, X., et al. (2022). Super-resolution Airy disk microscopy of individual color centers in diamond. ACS Photonics 9 (12), 3848–3854. doi:10.1021/acsphotonics.2c00713
- Greentree, A. D., Fairchild, B. A., Hossain, F. M., and Prawer, S. (2008). Diamond integrated quantum photonics. *Mater. Today* 11 (9), 22–31. doi:10.1016/S1369-7021(08)70176-7
- Hauf, M. V., Grotz, B., Naydenov, B., Dankerl, M., Pezzagna, S., Meijer, J., et al. (2011). Chemical control of the charge state of nitrogen-vacancy centers in diamond. *Phys. Rev. B* 83 (8), 081304. doi:10.1103/PhysRevB.83.081304
- Havlik, J., Petrakova, V., Rehor, I., Petrak, V., Gulka, M., Stursa, J., et al. (2013). Boosting nanodiamond fluorescence: towards development of brighter probes. *Nanoscale* 5 (8), 3208–3211. doi:10.1039/C2NR32778C
- Huang, L. C. L., and Chang, H.-C. (2004). Adsorption and immobilization of cytochrome c on nanodiamonds. *Langmuir* 20 (14), 5879–5884. doi:10.1021/la0495736
- Hui, Y. Y., Chen, O. Y., Azuma, T., Chang, B.-M., Hsieh, F.-J., and Chang, H.-C. (2019). Alloptical thermometry with nitrogen-vacancy centers in nanodiamond-embedded polymer films. *J. Phys. Chem. C* 123 (24), 15366–15374. doi:10.1021/acs.jpcc.9b04496
- Katsumi, R., Takada, K., Jelezko, F., and Yatsui, T. (2025). Recent progress in hybrid diamond photonics for quantum information processing and sensing. *Commun. Eng.* 4 (1), 85. doi:10.1038/s44172-025-00398-2
- Kidalov, S. V., Shakhov, F. M., and Ya Vul, A. (2007). Thermal conductivity of nanocomposites based on diamonds and nanodiamonds. *Diam. Relat. Mater.* 16 (12), 2063–2066. doi:10.1016/j.diamond.2007.07.010
- Kucsko, G., Maurer, P. C., Yao, N. Y., Kubo, M., Noh, H. J., Lo, P. K., et al. (2013). Nanometre-scale thermometry in a living cell. *Nature* 500 (7460), 54–58. doi:10.1038/nature12373
- Kumar, R., Singh, D. K., Kumar, P., Kumar, R., and Dhakate, S. R. (2019). Influence of degree of air oxidation and functionality on ensemble emission from nitrogen vacancy centers in nano-diamonds. *Diam. Relat. Mater.* 97, 107431. doi:10.1016/j.diamond. 2019.05.016
- Kumar, S., Nehra, M., Kedia, D., Dilbaghi, N., Tankeshwar, K., and Kim, K.-H. (2019). Nanodiamonds: emerging face of future nanotechnology. *Carbon* 143, 678–699. doi:10. 1016/j.carbon.2018.11.060
- Liu, W., Alam, Md N. A., Liu, Y., Agafonov, V. N., Qi, H., Koynov, K., et al. (2022). Silicon-vacancy nanodiamonds as high performance near-infrared emitters for live-cell dual-color imaging and thermometry. *Nano Lett.* 22 (7), 2881–2888. doi:10.1021/acs. nanolett.2c00040
- March, J. E., Wood, B. D., Stephen, C. J., Durán Fervenza, L., Breeze, B. G., Mandal, S., et al. (2023). Long spin coherence and relaxation times in nanodiamonds milled from polycrystalline $\{\{12\}$ $\$ unathrm $\{C\}$ diamond. *Phys. Rev. Appl.* 20 (4), 044045. doi:10. 1103/PhysRevApplied.20.044045
- Miller, B. S., Bezinge, L., Gliddon, H. D., Huang, D., Dold, G., Gray, E. R., et al. (2020). Spin-enhanced nanodiamond biosensing for ultrasensitive diagnostics. *Nature* 587 (7835), 588–593. doi:10.1038/s41586-020-2917-1

Mittiga, T., Hsieh, S., Zu, C., Kobrin, B., Machado, F., Bhattacharyya, P., et al. (2018). Imaging the local charge environment of nitrogen-vacancy centers in diamond. *Phys. Rev. Lett.* 121 (24), 246402. doi:10.1103/PhysRevLett.121. 246402

- Mosavian, N., Hubert, F., Smits, J., Kehayias, P., Silani, Y., Richards, B. A., et al. (2024). Super-resolution diamond magnetic microscopy of superparamagnetic nanoparticles. ACS Nano 18 (8), 6523–6532. doi:10.1021/acsnano.3c12283
- Neumann, P., Kolesov, R., Naydenov, B., Beck, J., Rempp, F., Steiner, M., et al. (2010). Quantum register based on coupled electron spins in a room-temperature solid. *Nat. Phys.* 6 (4), 249–253. doi:10.1038/nphys1536
- Neumann, P., Jakobi, I., Dolde, F., Burk, C., Reuter, R., Waldherr, G., et al. (2013). High-precision nanoscale temperature sensing using single defects in diamond. *Nano Lett.* 13 (6), 2738–2742. doi:10.1021/nl401216y
- Nie, L., Nusantara, A. C., Damle, V. G., Baranov, M. V., Chipaux, M., Reyes-San-Martin, C., et al. (2022). Quantum sensing of free radicals in primary human dendritic cells. *Nano Lett.* 22 (4), 1818–1825. doi:10.1021/acs.nanolett.1c03021
- Panich, A. M., Shames, A. I., Mogilyansky, D., Goren, S. D., and Yu Dolmatov, V. (2020). Detonation nanodiamonds fabricated from tetryl: synthesis, NMR, EPR and XRD study. *Diam. Relat. Mater.* 108, 107918. doi:10.1016/j.diamond.2020. 107918
- Peng, Z., Dallas, J., and Takahashi, S. (2020). Reduction of surface spin-induced electron spin relaxations in nanodiamonds. *J. Appl. Phys.* 128 (5), 054301. doi:10.1063/5.
- Perevedentseva, E., Lin, Y.-C., and Cheng, C.-L. (2021). A review of recent advances in nanodiamond-mediated drug delivery in cancer. *Expert Opin. Drug Deliv.* 18 (3), 369–382. doi:10.1080/17425247.2021.1832988
- Petráková, V., Taylor, A., Kratochvílová, I., Fendrych, F., Vacík, J., Kučka, J., et al. (2012). Luminescence of nanodiamond driven by atomic functionalization: towards novel detection principles. *Adv. Funct. Mater.* 22 (4), 812–819. doi:10.1002/adfm. 201101936
- Pezzagna, S., and Meijer, J. (2021). Quantum computer based on color centers in diamond. Appl. Phys. Rev. 8 (1), 011308. doi:10.1063/5.0007444
- Sangtawesin, S., Dwyer, Bo L., Srinivasan, S., Allred, J. J., H Rodgers, L. V., De Greve, K., et al. (2019). Origins of diamond surface noise probed by correlating single-spin measurements with surface spectroscopy. *Phys. Rev. X* 9 (3), 031052. doi:10.1103/PhysRevX.9.031052
- Schrand, A. M., Ciftan Hens, S. A., and Shenderova, O. A. (2009). Nanodiamond particles: properties and perspectives for bioapplications. *Crit. Rev. Solid State Mater. Sci.* 34 (1-2), 18–74. doi:10.1080/10408430902831987
- Stehlik, S., Varga, M., Ledinsky, M., Jirasek, V., Artemenko, A., Kozak, H., et al. (2015). Size and purity control of HPHT nanodiamonds down to 1 nm. *J. Phys. Chem. C* 119 (49), 27708–27720. doi:10.1021/acs.jpcc.5b05259
- Tegafaw, T., Liu, S., Ahmad, M. Y., Saidi, A. K. A., Zhao, D., Liu, Y., et al. (2023). Production, surface modification, physicochemical properties, biocompatibility, and bioimaging applications of nanodiamonds. *RSC Adv.* 13 (46), 32381–32397. doi:10.1039/D3RA06837D
- Tsukahara, R., Fujiwara, M., Sera, Y., Nishimura, Y., Sugai, Y., Jentgens, C., et al. (2019). Removing non-size-dependent electron spin decoherence of nanodiamond quantum sensors by aerobic oxidation. *ACS Appl. Nano Mater.* 2 (6), 3701–3710. doi:10.1021/acsanm.9b00614
- Volkov, K. V., Danilenko, V. V., and Elin, V. I. (1990). Synthesis of diamond from the carbon in the detonation products of explosives. *Combust. Explos. Shock Waves* 26 (3), 366–368. doi:10.1007/BF00751383
- Wang, X., Cao, W., Su, Z., Zhao, K., Dai, B., Gao, G., et al. (2023). Fabrication of high thermal conductivity nanodiamond/aramid nanofiber composite films with superior multifunctional properties. *ACS Appl. Mater. and Interfaces* 15 (22), 27130–27143. doi:10.1021/acsami.3c02574
- Wolcott, A., Schiros, T., Trusheim, M. E., Chen, E. H., Nordlund, D., Diaz, R. E., et al. (2014). Surface structure of aerobically oxidized diamond nanocrystals. *J. Phys. Chem. C* 118 (46), 26695–26702. doi:10.1021/jp506992c
- Wu, Y., Balasubramanian, P., Wang, Z., Coelho, J. A. S., Prslja, M., Siebert, R., et al. (2022). Detection of few hydrogen peroxide molecules using self-reporting fluorescent nanodiamond quantum sensors. *J. Am. Chem. Soc.* 144 (28), 12642–12651. doi:10.1021/jacs.2c01065
- Zhai, M.-jie, Zhang, F.-lin, Chen, X.-sen, Lin, Y.-bin, Zhu, M.-xing, Tang, H.-qun, et al. (2021). Preparation and characterization of nanodiamond reinforced aluminum matrix composites by hot-press sintering. *Diam. Relat. Mater.* 120, 108664. doi:10.1016/j.diamond.2021.108664
- Zhang, B., Feng, X., Yin, H., Ge, Z., Wang, Y., Chu, Z., et al. (2017). Anchored but not internalized: shape dependent endocytosis of nanodiamond. *Sci. Rep.* 7 (1), 46462. doi:10.1038/srep46462
- Zhang, T., Ma, L., Wang, L., Xu, F., Wei, Q., Wang, W., et al. (2021). Scalable fabrication of clean nanodiamonds via salt-assisted air oxidation: implications for sensing and imaging. ACS Appl. Nano Mater. 4 (9), 9223–9230. doi:10.1021/accept. 101751